Andrej Predin
University of Maribor
Smetanova 17, SI-2000
Maribor, Slovenia

Torsional Vibrations at Guide-Vane Shaft of Pump–Turbine Model

This article focuses on the problem of guide-vane vibrations of reversible pump–turbines, especially, in the pump mode. These vibrations are transmitted to the guide-vane shaft torque. The guide-vane vibrations are caused by the impeller exit flow, which has a turbulent and partly nondeterministic property. Experimentally determined flow velocities at the impeller exit are given. The mathematical models for theoretical torsional vibration prediction formulated using linear and nonlinear differential equations are presented. The results of theoretical calculations are compared with measurement results. The possibility of transferring the parameters from the model to the prototype is discussed.

INTRODUCTION

When a pump is operating at partial load, the fluid flow at the impeller is characterized by a period pressure, especially at smaller output capacities. These flow pressure pulsations are transmitted to flow velocities and have a periodic pulse shape. The flow excites oscillations of the guide vane (GV). A small nonlinearity exists in the GV torsional vibrations caused by flow turbulence. For the optimization of GV profiles and the shaft location, the flow pulsation properties (load), dynamic behavior of the GV (structural vibrations), and its coupling effect must be known. In major cases the shaft diameter is limited by the GV profile thickness.

Testing Pump-Turbine Model System and GV Torque Measurement System

The experimental system consists of a driving part, simplified pump–turbine model (SPTM), and entrance pipe system (Fig. 1a). It is installed in the Laboratory for Turbine Machines at the Faculty of Mechanical Engineering, University of Maribor. The SPTM radial impeller has a constant width (b_2) and 11 cylindrical blades ($z_i = 11$). The guide apparatus of the SPTM has 24 GVs ($z_{GV} = 24$), 12 stay vanes ($z_{SV} = 12$), and a volute casing on the exit (Fig. 1b). The system for GV torque measurement (Fig. 2) is based on the elastic torsion distortion measurements at the thin wall of the GV shaft. At this location the strain gauge strips (HBM LY13) are bonded. The strips are connected into the full Wheatstone bridge. This strip connection allows the temperature compensation. The strips are placed enclosed in the shaft axis at an angle of 45° to the shaft axis, because in this direction the main torsional stress effects are found. In this way, the bending stresses are also partly compensated. (The shaft is fixed as a cantilever beam with one axial support point on the opposite side.) The measurement system is calibrated using weights each time before measuring.

Received May 25, 1995; Accepted December 15, 1996.
Shock and Vibration, Vol. 4, No. 3, pp. 153–162 (1997)

CCC 1070-9622/97/030153-10

a)

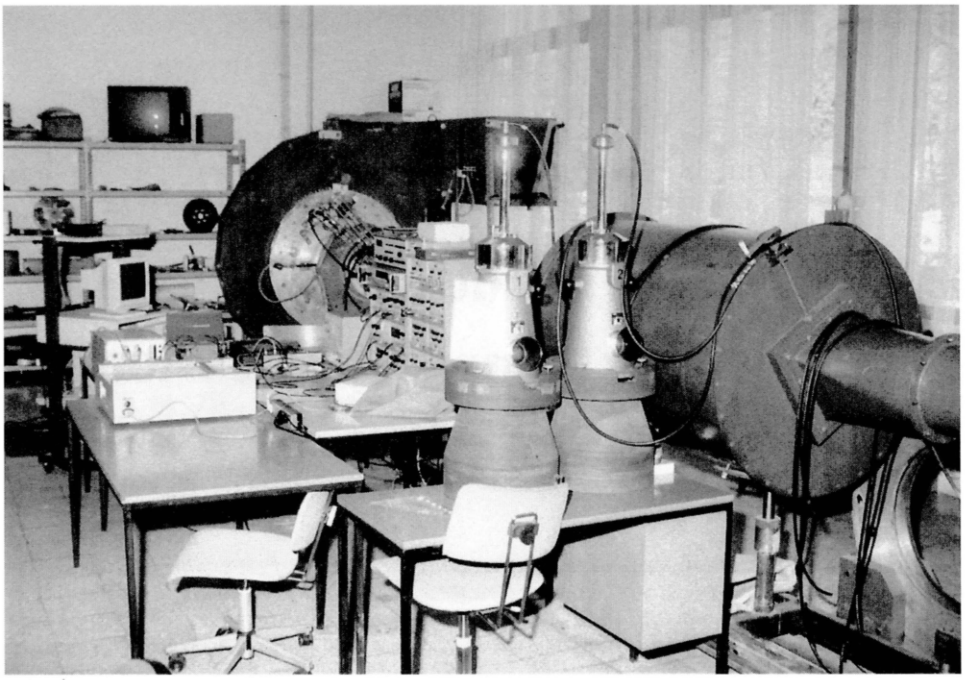

b)

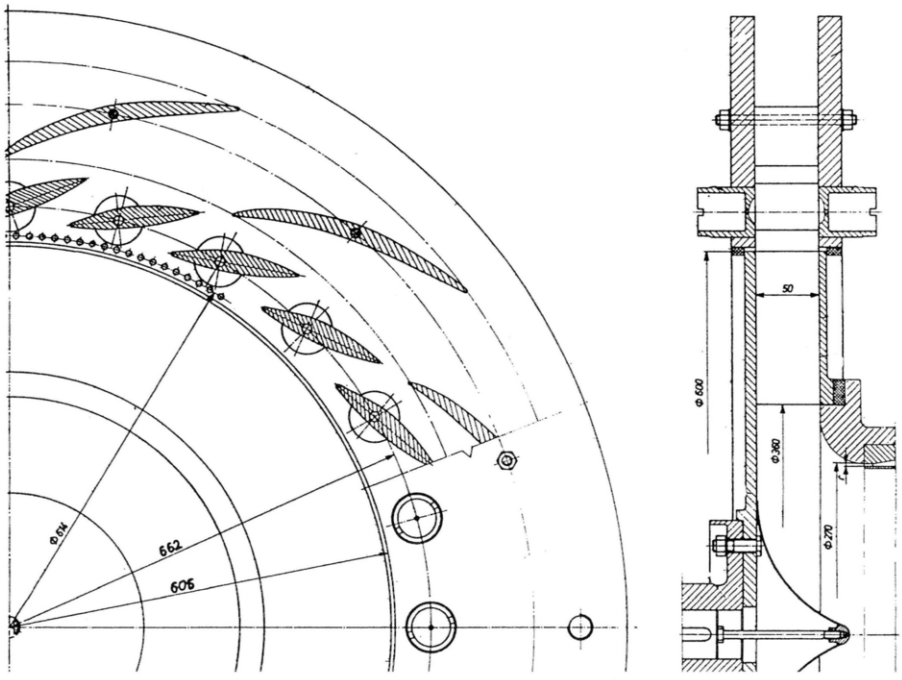

FIGURE 1 (a) Testing model system and (b) simplified pump-turbine model.

The response is almost linear and the calibration response repetition is satisfactory. The measurement system natural (eigen) frequency and its damping coefficient are determined by impulse response (free decay method). The natural frequency is lower than the flow pulsation frequency.

FLOW VELOCITIES AT IMPELLER EXIT

The flow pulsation at the impeller exit could be caused by the relative circulation flow at the individual impeller channel. This circulation flow can be represented by relative flow velocities. Super-

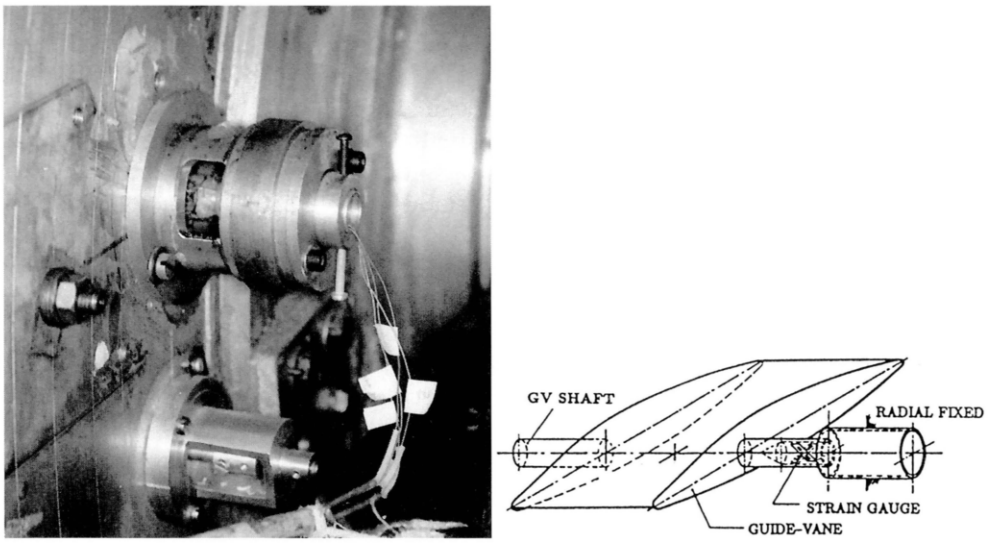

FIGURE 2 Measurement system for guide-vane torque measurement.

position of flows through the impeller increases the relative velocity at the lower surfaces of the blade and reduces the velocity at the upper surface of the blade (back curved impeller blade). The result is a component in the tangential direction (B–B') opposite to the absolute flow velocity component in the tangential direction c_{u2} at the discharge (Fig. 3a) and an additional component (D–D') in the direction of c_{u1} at the impeller channel entrance (Fig. 3b). A study of velocity components of discharge velocity triangles (Fig. 3) will reveal that the relative circulation of fluid within the impeller blades has the effect of decreasing the flow discharge angle from blade angle β_2 to β_2' and absolute flow velocity angles at discharge α_2 to α_2', respectively. This means that the flow velocities at the impeller discharge pulsate in an absolute direction and in the direction of the flow velocity angle. The flow pulsation frequency is determined by

$$f_f = n_i z_i, \tag{1}$$

where n_i is the impeller rotation speed and z_i is the number of the blade. Reynolds' idea was to separate flow velocities into its mean and fluctuation components. Therefore, the instantaneous flow velocity at the impeller exit can be determined as

$$U = \overline{U} + u, \tag{2}$$

where $U(c_u, c_m)$ is the flow velocity plane function, $\overline{U}$ is its mean value, and u is its fluctuation value. The overscore denotes the average value of the fluctuation velocities, so by definition

$$\begin{aligned} u' &= u - \overline{u}, \\ \overline{u}' &= \frac{1}{T}\int_0^T (u - \overline{u})\, dt = \overline{u} - \overline{u} = 0, \end{aligned} \tag{3}$$

which allows the possibility of averaging the absolute values of the fluctuation velocities. The non-

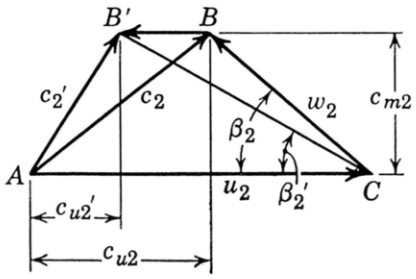

a)

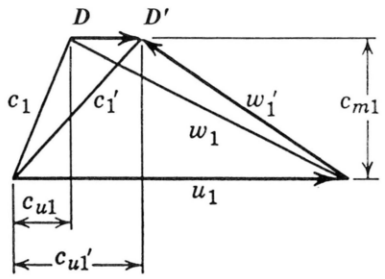

b)

FIGURE 3 (a) Discharge velocity triangle and (b) entrance velocity triangle.

Table 1. Relative Flow Turbulence Intensity

Q/Q_{opt}	0.15	0.77	1.00	1.23
Ti	0.31	0.17	0.13	0.17

zero value of the turbulence fluctuations is determined as the root mean square value,

$$u' = \sqrt{\overline{u}^2}. \tag{4}$$

The relative intensity is defined by the ratio

$$Ti = \frac{u'}{\overline{U}}. \tag{5}$$

The mean value for the time average turbulence is determined by

$$\overline{U} = \lim_{T\to\infty} \frac{1}{2T} \int_{-T}^{T} U\, dt, \tag{6}$$

where T is the average time. The turbulence intensity is

$$Ti = \frac{1}{c} \sqrt{\frac{1}{2}(c_u'^2 + c_m'^2)}, \tag{7}$$

where c is $\sqrt{c_u^2 + c_m^2}$, and c_u', c_m' are fluctuations of absolute flow velocity in the tangential and meridian direction. The relative flow turbulence intensity values are given at four capacities (Table 1).

By increasing the capacity up to the optimal capacity (the capacity at the best efficiency operating point), the flow pulsation amplitudes declined. With a further capacity increase over the optimal capacity, the pulsation flow amplitudes again increased. The flow velocities were measured at the impeller exit by an anemometer system (DISA 55M) with a one channel hot wire probe (DISA 55P11). The measurement points at the measurement diameter D_{3m} are arranged by 2° at the impeller exit (Fig. 4). The flow velocities are measured in absolute, meridian, and tangential directions at the apparent streamlines at the impeller width ($b_2/2$). The flow velocities are given in the tangential direction in nondimensional form,

$$\psi = \frac{c_{u2}}{u_2}, \tag{8}$$

by head coefficient ψ in the time-history record (Fig. 5a). The absolute flow velocity angle α_2 is given in a nondimensional form

$$k_\alpha = \frac{\alpha_2}{\alpha_{2,th}}, \tag{9}$$

where $\alpha_{2,th}$ is the theoretically determined exit flow velocity angle of absolute velocity c_2, in the time-history record as well (Fig. 5b). Pulsation head coefficient and exit flow angle are evident from the time-history records (Fig. 5). The frequency of velocity measurements data is exactly equal to

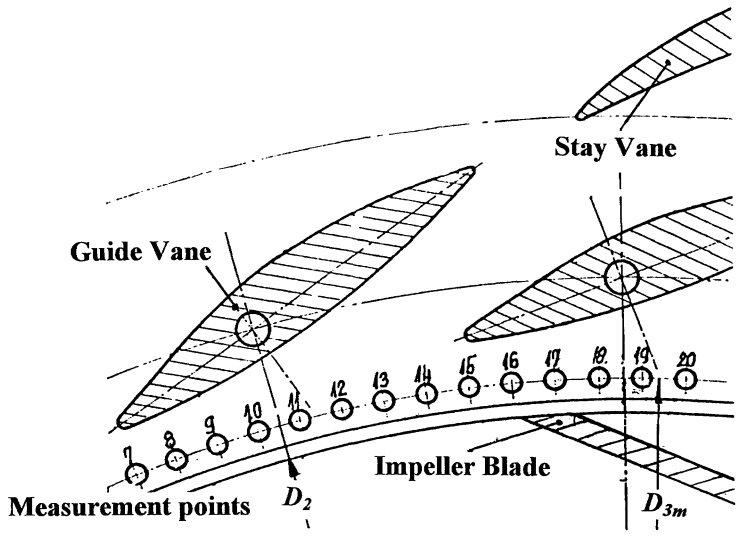

FIGURE 4 Measurement sector-measurement points on diameter D_{3m}.

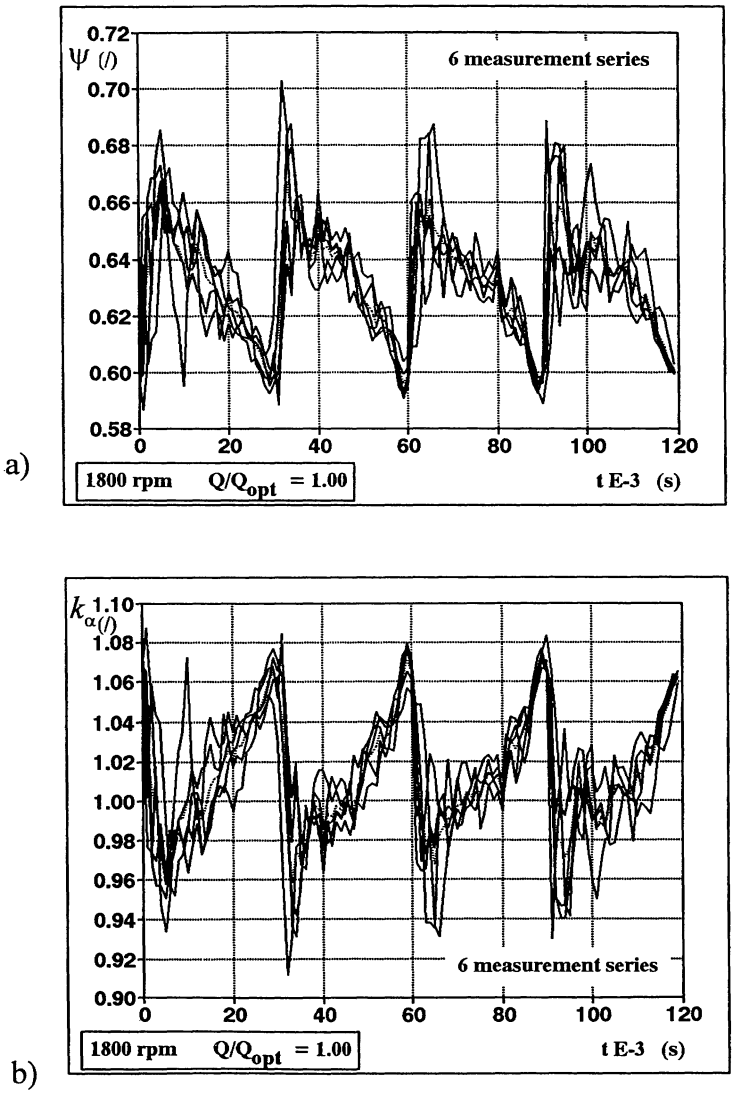

FIGURE 5 (a) Time history record of heat coefficient and exit (b) flow velocity angle coefficient.

the flow pulsation frequency (forced blade passage frequency), which is determined by Eq. (1). The pulsation amplitude is decreased by increasing capacity up to the optimal capacity. This is evident from power spectra records (Fig. 6). The flow pulsation amplitudes increase again when the capacity increases over the optimal capacity. This is probably a consequence of prerotation flow in the entrance pipe. Under optimal capacities the prerotation flow has the same direction as the impeller rotation. At optimal capacity the prerotation flow is zero, and over optimal capacity the prerotation flow has the opposite direction with respect to the impeller rotation.

Torque at the GV Shaft

Torque at the GV shaft is a consequence of the hydrodynamic force acting on the GV profile. The pulsating GV torque could be expected, because the flow has a pulsating and partly turbulent nature (especially in pump operation mode). This can be resolved into three basic components: mean or static torque, pulsation or oscillation deterministic torque, and nondeterministic or stochastic torque. The mean torque part is measured and the signal is averaged (t = 3 s) at different capacities. The pulsation torsional oscillations arise because of the flow induced GV vibrations. These torsional oscil-

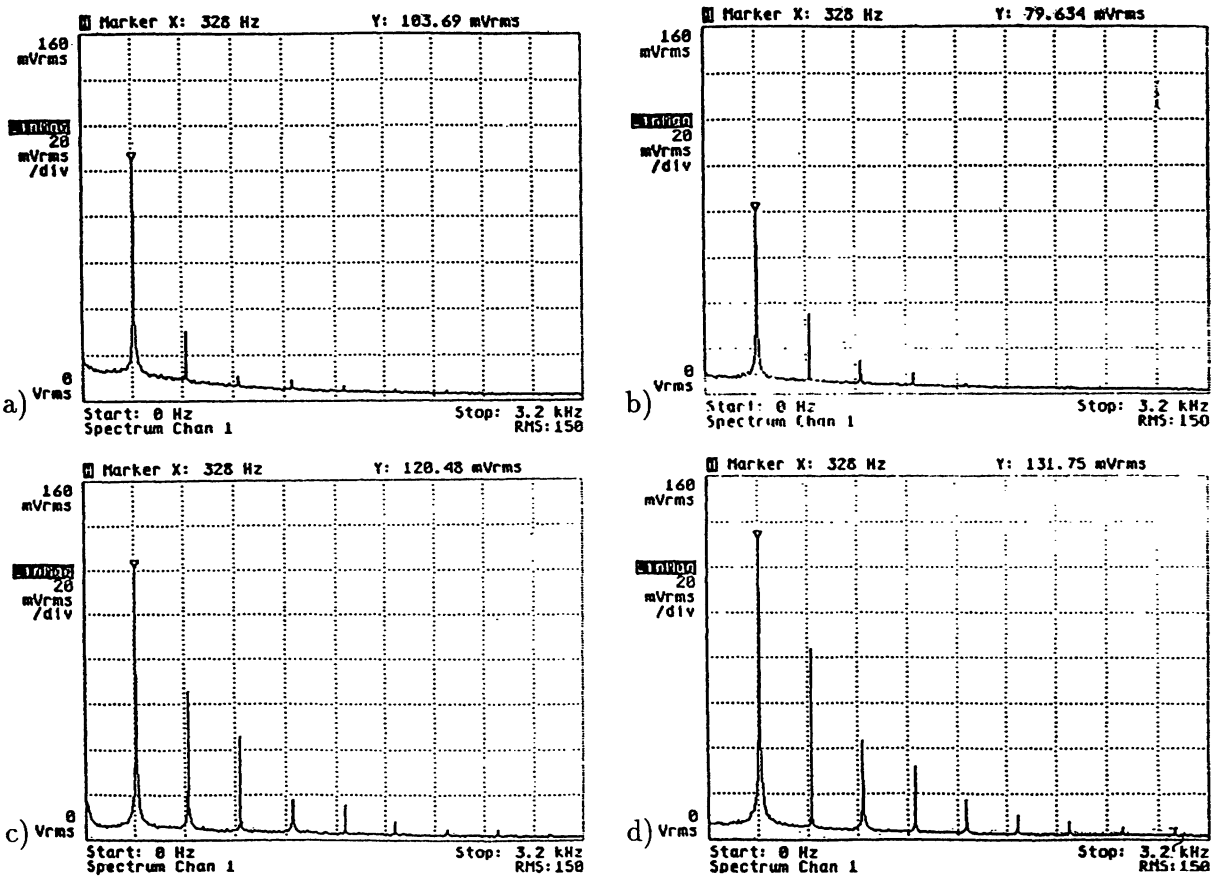

FIGURE 6 Power spectra records of absolute flow velocity c_{2u} for capacity ratios: $Q/Q_{opt} = 0.15$ (a), $Q/Q_{opt} = 0.77$ (c), $Q/Q_{opt} = 1.00$ (b) and $Q/Q_{opt} = 1.23$ (d).

lations can be treated separately: first, as GV vibrations induced by a relatively uniform flow (turbine operating mode) and second, as pulsating flow induced GV oscillations (pump operating mode). The stochastic torsion oscillation is a consequence of flow turbulence present in turbine and pump operating modes. The pulsation and stochastic GV torsion oscillations constitute the vibrating time varying torque. The pulsation GV shaft torque is measured using an A/D board. The sampling time is 0.0001667 s per channel. Six measurement series data are given in a time-history form as a function of the model operating capacity (Fig. 7). The torque amplitudes are normalized with respect to the maximal amplitude (A/A_{max}). The maximal amplitude is measured at minimal capacity ($Q/Q_{opt} = 0.15$).

The basic equation of motion governing torsional oscillation with damping is

$$J_\Theta \ddot{\Theta} + 2J_\Theta \xi_\Theta \dot{\Theta} + k_\Theta \Theta = F(t), \qquad (10)$$

where $F(t)$ is the external excitation, k_Θ represents the stiffness of the shaft material, ξ_Θ is a damping coefficient, and J_Θ denotes the torsional moment of inertia of the measurement system (GV with shaft). As mentioned before, the GV torque vibrations in the turbine operation mode have to be treated as flow induced vibrations in the relatively uniform flow. Equation (10) can be rearranged for turbine operation mode as

$$J_\Theta \ddot{\Theta} + 2J_\Theta \xi_\Theta \dot{\Theta} + k_\Theta \Theta = a\frac{1}{2}\rho c^2 L c_L, \qquad (11)$$

where J_Θ denotes the torsional moment of inertia of the GV, Θ is the torsional oscillation angle distortion, k_Θ represents the GV shaft material stiffness coefficient, L is the foil (GV profile) chord, c_L is the lift coefficient, and a is the distance between the point where the hydrodynamic force is applied (in the direction of the foil chord) and the GV shaft axis. Divergence or stability velocity of

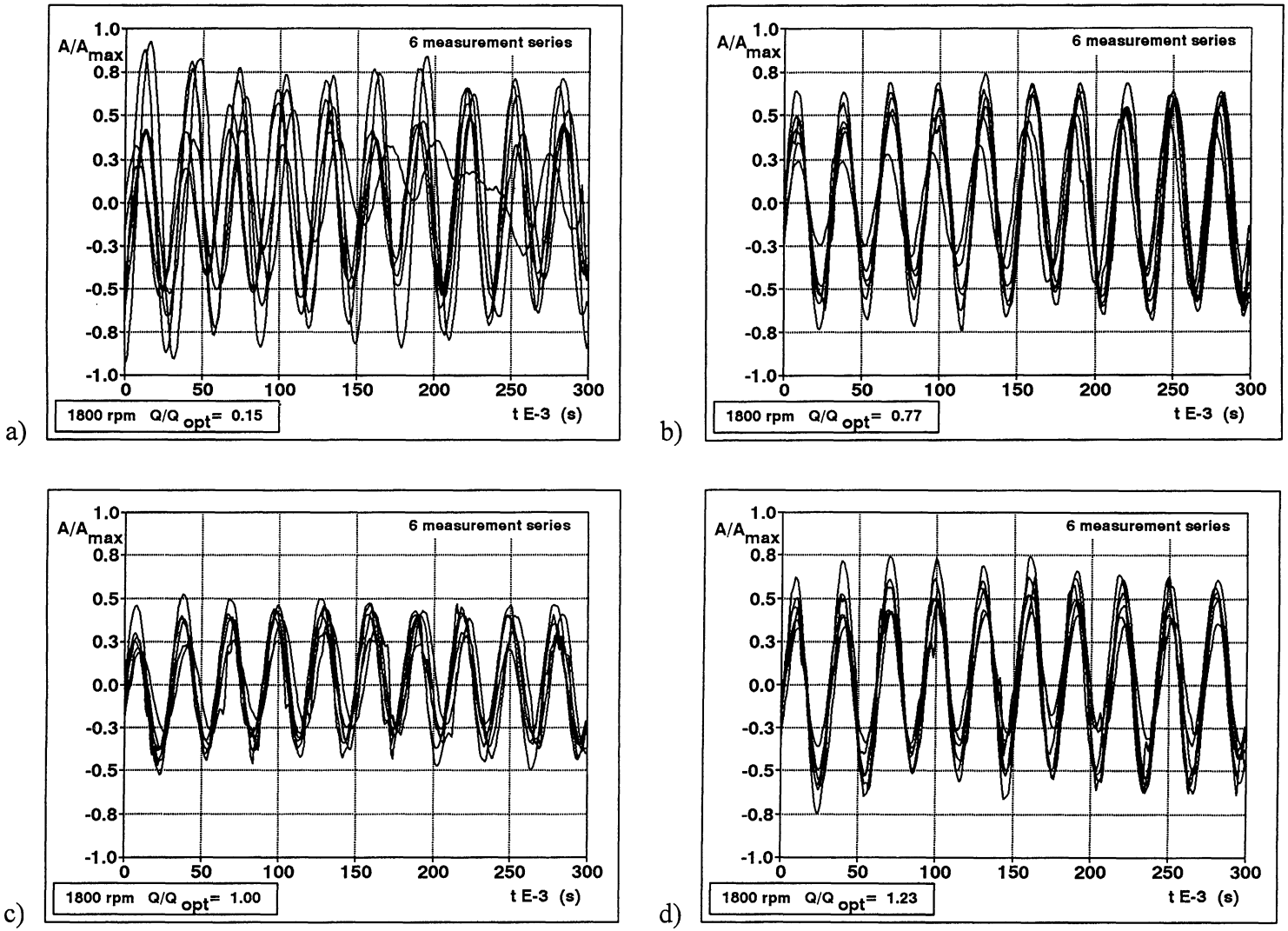

FIGURE 7 Time-history records of pulsation torque at different operating capacities.

an airplane wing foil (Blevins, 1990) occurs where the flow velocities are much larger than the flow velocities of a spiral volute pump–turbine. This is the reason that the probability of GV oscillation in turbine operation mode is very low. But, as an exact study of flow in the turbine operating mode shows, the flow is not uniform, because the runner has an influence on the flow in the guide apparatus. This is especially reflected in the boundary layer on the GV surface (Fisher et al., 1994).

In the pump operation mode the GV vibrations must be treated as pulsating flow induced vibrations. The simple mathematical model can be expressed by Eq. (10) and represents rigid-body forced oscillations,

$$J_\Theta \ddot{\Theta} + 2J_\Theta \xi_\Theta \dot{\Theta} + k_\Theta \Theta = A_{atp} \cos \omega t, \quad (12)$$

where A_{atp} is the amplitude of the alternating torque part. The results obtained using this model are given in a publication by Predin and Popovič (1993) and with respect to the flow turbulence in an article by Predin and Popovič (1994). But these mathematical models do not treat the GV vibrations as a coupled problem between a rigid-body oscillation and flow pulsation. So, in pump operating mode, the GV vibrations must be treated as a coupled problem between solid structure oscillation and fluid flow pulsation. In Eq. (11) the pulsation flow velocities absolute flow velocity at the impeller exit are considered in the following form:

$$c = c_2 + c_{2,p} \cos \omega t. \quad (13)$$

In Eq. (13) $c_{2,p}$ is the flow velocity pulsation amplitude. By inserting Eq. (13) into Eq. (11) we have

$$J_\Theta \ddot{\Theta} + 2J_\Theta \xi_\Theta \dot{\Theta} + k_\Theta \Theta = a \frac{1}{2} \rho c^2 L c_L (c_2 + 2c_2 c_{2,p} \cos \omega t + c_{2,p}^2 \cos^2 \omega t). \quad (14)$$

By introducing new constants (λ_I, λ_{II}), Eq. (14) can be rewritten as

$$\ddot{\Theta} + 2\xi_\Theta \dot{\Theta} + \frac{k_\Theta}{J_\Theta} \Theta = \lambda_I + \cos \omega t + \lambda_{II} \cos^2 \omega t. \quad (15)$$

The first term on the right side contributes only to the static part of torsional oscillations and can be neglected. Equation (15) can be rearranged into the following system of equations:

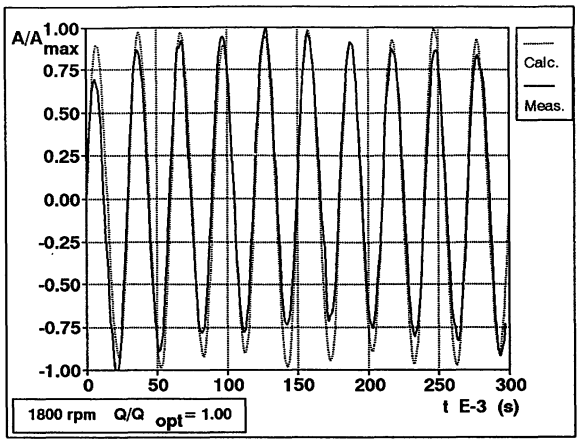

FIGURE 8 Time history record of pulsation torque compared to theoretical results of mathematical model, Eq. (15).

$$\ddot{\Theta} + 2\xi_\Theta \dot{\Theta} + \frac{k_\Theta}{J_\Theta} \Theta = 0, \quad (16a)$$

$$\ddot{\Theta} + 2\xi_\Theta \dot{\Theta} + \frac{k_\Theta}{J_\Theta} \Theta = \cos \omega t, \quad (16b)$$

$$\ddot{\Theta} + 2\xi_\Theta \dot{\Theta} + \frac{k_\Theta}{J_\Theta} \Theta = \lambda_{II} \cos^2 \omega t, \quad (16c)$$

where λ_{II} is a constant proportional to the ratio of mean flow velocity and pulsation flow velocity amplitude. The complete solution of equation system (16) is the sum of the individual solutions of Eq. (16a–c):

$$\Theta(t) = \Theta_a(t) + \Theta_b(t) + \Theta_c(t). \quad (17)$$

Figure 8 shows a good correlation between Eq. (17) results and experimental results. In this sum of solutions (17) the first higher harmonic of flow (forced) frequency is also considered. By classic treatment, considering only the rigid-body oscillation, this higher harmonic can be overlooked. With initial conditions taking into account the flow turbulence,

$$\begin{aligned} \Theta_s - Ti \le \Theta_0 \le \Theta_s + Ti, \\ \dot{\Theta}_s - Ti \le \dot{\Theta}_0 \le \dot{\Theta}_s + Ti, \end{aligned} \quad (18)$$

we get satisfactory results in the sense of nondeter-

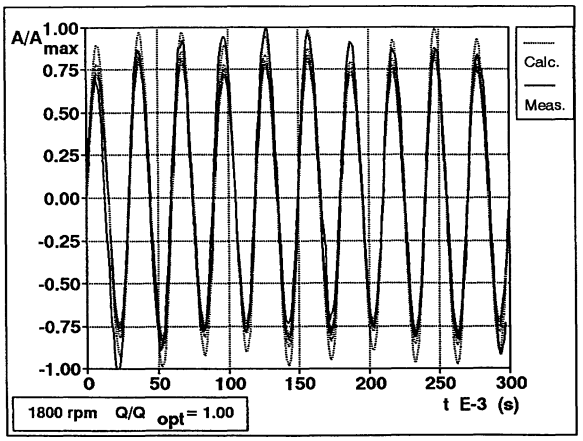

FIGURE 9 Time history record of pulsation torque compared to theoretical results for mathematical model, Eq. (15), considering flow turbulence.

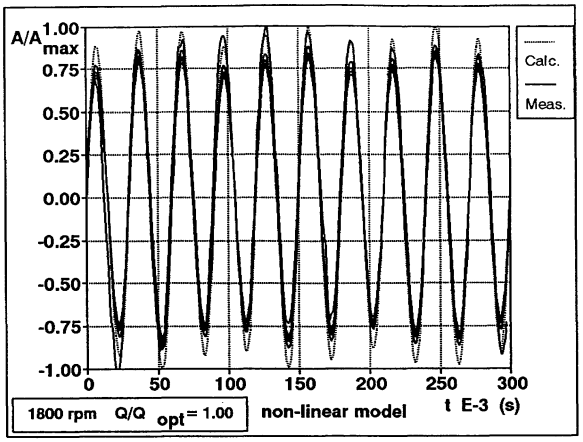

FIGURE 10 Time history record of pulsation torque compared to theoretical results of mathematical model, Eq. (21), considering flow turbulence.

ministic pulsation torque changes (Fig. 9). Obvious stationary GV oscillations are created after approximately 900 impeller rotations; this corresponds to a start time (t = 45 s) at the impeller at 1800 rpm. The natural GV oscillations in complete GV vibrations are not dominant. Their influence is relatively small for stationary oscillations. The reason why the GV oscillation or its amplitudes do not reach the resonant condition, even under synchronous flow excitation, can be explained by the nature of the fluid flow. The fluid flow at the impeller exit simultaneously excites and damps GV vibrations with respect to the flow conditions (absolute flow velocities and its angle changes). To consider this fact the variable system damping factor is dependent on the torsional distortion angle,

$$\xi_p = \zeta_\Theta \cos \Theta, \tag{19}$$

where ξ_Θ = 0.00577 N s/m and $\xi = \xi_\Theta/\xi_{\Theta,cr}$ = 0.04. Equation (15) can be expanded into the nonlinear differential equation, by considering damping factor as an angle Θ function:

$$\ddot{\Theta} + 2(\xi_\Theta \cos \Theta)\dot{\Theta} + \frac{k_\Theta}{J_\Theta}\Theta = \lambda_I + \cos \omega t + \lambda_{II} \cos^2 \omega t. \tag{20}$$

The results (Fig. 10) of this nonlinear mathematical model, Eq. (20), using a numerical integration method, are similar to the linear solutions. This is a consequence of a relatively small system damping coefficient, which has a small influence on the dominant forced oscillations in GV vibrations. Anyway, a nonlinear mathematical model is much more sensitive to the initial conditions than the linear model, because the natural GV oscillation depends on damping and start time.

This small nonlinearity, which is taken into account in the differential equation by the variable damping coefficient depending on angle Θ, is too small to cause any nonstable GV torsional vibrations. The GV vibrations remain stable.

VIBRATION PARAMETER TRANSFER FROM MODEL TO PROTOTYPE

Complete mapping of all parameters from model to prototype is practically impossible. It is very difficult to reach even Reynolds number equality, especially when the model operates in air and the prototype in water. The geometric similarity between the model and prototype can be easily reached, because only the length scale must be equal (Buckingham's Π theorem; Shames, 1992). In the case of the above given GV vibration, we must proceed from the coupled effect of rigid-body oscillations and flow pulsation, or by considering hydroelastic vibrations. Flow similarity is considered in the so-called Strouhal similarity, which is treated in whirl flow frequency mapping (Jacob, 1994) on the GV surface. The Strouhal number, which can be determined from the Froude number equality and kinematic similarity, is

$$\mathrm{St} = \frac{\omega L}{c_2} = \frac{2\pi f L}{c_2} = \frac{\omega d}{2\pi c} = \frac{fd}{c_2}, \tag{21}$$

where d is the hydraulic diameter of the GV. Equation (21) can be used for mapping the "third torque part" (effect of flow turbulence), where f represents the frequency of rising whirls in the boundary layer on the GV surface. Basic, or forced, frequency ("second torque part") of flow pulsation, or its influence on GV oscillations, can be mapped directly from the frequency ratio

$$\frac{f_{0,m}}{f_{0,p}} = \frac{z_{i,m} n_m}{z_{i,p} n_p} \tag{22}$$

between the model and prototype, and similarity of the natural frequencies of GVs, with

$$\frac{f_{n,m}}{f_{n,p}} = \frac{k_m}{k_p} \sqrt{\frac{E_m \rho_p}{E_p \rho_m}}, \tag{23}$$

where k_m and k_p are the stiffness of the GV shaft of model and prototype; E_m and E_p are the Young's modulus for the shaft material of the model and prototype, and ρ_m and ρ_p are the densities of the GV and shaft material of the model and prototype.

CONCLUSIONS

By considering the GV oscillations and fluid flow pulsations as a coupled problem, the first higher harmonic of forced frequency can be treated in common GV vibrations. The higher harmonic is neglected by treating the GV vibrations as rigid-body oscillations. In the experimentally determined frequency spectrum record, this forced frequency first higher harmonic is present. Estimation of this higher harmonics frequency amplitude equivalent to the ratio between the mean and pulsation velocities gives a good approximation for amplitude determination.

The linear mathematical models results correlate well with the experimental measurement results by use of the turbulent coefficient in initial conditions of differential equations, by frequency response, and in oscillation forms in the sense of nondeterministic individuality of repetition measurements.

The results of the nonlinear mathematical model do not differ significantly from the linear model results. This is a consequence of the small damping coefficient, and the small influence of the natural oscillation on common GV oscillation in stationary conditions.

Changeable fluid flow angle at the impeller exit and changeable system damping limits the GV oscillation amplitudes so that they stay finite, even by synchronic GV excitation by pulsation flow.

When considering the starting time in presented theoretical forms of GV torsional oscillations (t = 45 s), the small influence of natural oscillation on common GV oscillation is evident. This condition shows that the steady-state GV oscillation after the start time after 900 impeller rotations is restored. This is also confirmed by measurements.

The presented hydrovibration parameter transfer from model to prototype may be used to obtain satisfactory results in predicting the influence of GV oscillations on the operating behavior of pump–turbines.

REFERENCES

Blevins, R. D., 1990, *Flow-Induced Vibration,* 2nd ed., Van Nostrand Reinhold, New York.

Fisher, R. K., Grummer, J. H., and Liess, C., 1994, "Stay Vane Vibrations in the Nkula Falls Turbines," *The International Journal on Hydropower & Dams,* Vol. 1, pp. 15–20.

Jacob, T., 1994, "Similitudes in Stability of Operation Test for Francis Turbines," *The International Journal on Hydropower & Dams,* Vol. 1, pp. 27–31.

Predin, A., and Popovič, M., 1993, "Contribution to the Measurements and Analysis of Pulsatory Hydrodynamic Force and Their Torque on Guide-Vanes of the Turbine–Pump Systems," *Proceedings of the 13th IMECO Conference on Force and Mass Measurement,* IMECO Technical Committee Series 31, Helsinki, Finland, pp. 137–144.

Predin, A., and Popovič, M., 1994, "Torque Vibrations at the Guide-Vane Shaft of the Pump–Turbine Model," *Proceedings of the 65th Shock and Vibration Symposium,* San Diego, CA, pp. 437–446.

Shames, I. H., 1992, *Mechanics of Fluids,* 3rd ed., McGraw–Hill, New York.